DOI: 10.1002/cctc.201100275

# Nitrogen- and Oxygen-Functionalized Multiwalled Carbon Nanotubes Used as Support in Iron-Catalyzed, High-Temperature Fischer–Tropsch Synthesis

Hendrik J. Schulte, Barbara Graf, Wei Xia, and Martin Muhler*[a]

High-temperature Fischer–Tropsch synthesis for the production of short-chain olefins over iron catalysts supported on multiwalled carbon nanotubes (CNTs) was investigated under industrially relevant conditions (340 °C, 25 bar, $H_2/CO = 1$) to elucidate the influence of nitrogen and oxygen functionalization of the CNTs on the activity, selectivity, and long-term stability. Surface functionalization of the CNTs was achieved by means of a gas-phase treatment using nitric acid vapor at 200 °C for oxygen functionalization (O-CNTs) and ammonia at 400 °C for the subsequent nitrogen doping (N-CNTs). Ammonium iron citrate impregnation followed by calcination was applied for the deposition of iron nanoparticles with particle sizes below 9 nm. Subsequent to reduction in pure $H_2$ at 380 °C, the Fe/N-CNT and Fe/O-CNT catalysts were applied in Fischer–Tropsch synthesis, in which they showed comparable initial conversion values with an excellent olefin selectivity [$S(C_3–C_6) > 85\%$] and low chain growth probability ($\alpha \leq 0.5$). TEM analysis of the used catalysts detected particle sizes of 23 and 26 nm on O-CNTs and N-CNTs, respectively, and $Fe_5C_2$ was identified as the major phase by using XRD, with only traces of $Fe_3O_4$. After 50 h time on stream under steady-state conditions, an almost twofold higher activity compared to the Fe/O-CNT catalysts had been maintained by the Fe/N-CNT catalysts, which are considered excellent Fischer–Tropsch catalysts for the production of short-chain olefins owing to their high activity, high selectivity to olefins, low chain growth probability, and superior long-term stability.

## Introduction

Fischer–Tropsch synthesis (FTS) is a well-established industrial process for converting synthesis gas derived from coal, natural gas, or biomass over iron or cobalt catalysts into mainly linear hydrocarbons exhibiting a broad chain-length distribution. Owing to the high volatility of the crude oil price over the past years and severe environmental regulation, FTS over cobalt- and iron-based catalysts has attracted increasing industrial attention. It represents an alternative reaction pathway to produce both high-quality fuels without sulfur or aromatic compounds and petrochemical commodities.[1–3] High synthesis temperatures and iron-based catalysts are essential for short-chain $\alpha$-olefins.[4]

Unsupported and also supported catalysts have been applied in FTS. For the supported catalysts, the catalytic activity and selectivity were influenced by the properties of the support materials (such as silica, alumina, and titania), the metal dispersion and loading, and the preparation method.[5,6] Vannice and co-workers[7–11] investigated iron catalysts supported on active carbon and reported a higher activity per unit volume and higher olefin selectivity compared to those of unsupported catalysts. Considering these catalytic benefits and the unique properties of carbon nanotubes (CNTs), such as high thermal conductivity and chemical stability, CNTs can be expected to be a superior catalyst support for the FTS. Indeed, Steen and Prinsloo[12] showed that iron supported on CNTs is active in FTS. Prior to iron deposition, they activated the initially inert CNT surfaces with nitric acid to generate oxygen-containing functional groups, which act as anchoring sites for iron nanoparticles. Unfortunately, Steen and Prinsloo's catalyst underwent strong deactivation during time on stream, and the expected increase in olefinicity was not observed. Therefore, subsequent studies focused mainly on catalyst stabilization. Bahome et al.[13,14] reported on iron deposition using incipient wetness as well as precipitation techniques on CNTs grown over an iron catalyst supported on $CaCO_3$. Catalytic testing showed no catalyst deactivation for all catalysts at comparable reaction conditions, and docking stations formed by etching with residual Ca during the surface activation were found to stabilize iron nanoparticles.[13,14] Bao and co-workers,[15] as well as Dalai and co-workers,[16] achieved the deposition of iron nanoparticles either inside or outside of the CNTs. In both studies the deactivation behavior was more pronounced for iron nanoparticles located on the exterior surface of the tubes, whereas those located inside the CNTs were found to be stabilized.

In all these studies, the surface activation by nitric acid was used to generate oxygen-containing functional groups on the CNTs. Recently, Chetty et al.[17] activated CNTs by means of a nitrogen plasma treatment, which resulted in nitrogen anchors for metal deposition. They found a significantly higher activity for nitrogen-anchored PtRu catalysts in electrochemical

[a] H. J. Schulte, Dr. B. Graf, Dr. W. Xia, Prof. Dr. M. Muhler
Laboratory of Industrial Chemistry
Ruhr-University Bochum
Universitätsstraße 150, 44780 Bochum (Germany)
E-mail: muhler@techem.rub.de

methanol oxidation compared to oxygen-activated CNTs. Coville and co-workers[18] observed higher activities and stabilities for a Co FTS catalyst supported on nitrogen-doped carbon spheres.

To the best of our knowledge, iron nanoparticles deposited on oxygen-functionalized CNTs (O-CNTs) and nitrogen-functionalized CNTs (N-CNTs) have not yet been compared under high-temperature FTS conditions. The CNTs were first exposed to nitric acid vapors and then to ammonia, followed by iron deposition using impregnation with ammonium iron citrate. Catalytic testing under industrially relevant conditions was used to demonstrate the unique properties of O-CNTs and N-CNTs for the iron-catalyzed, high-temperature FTS.

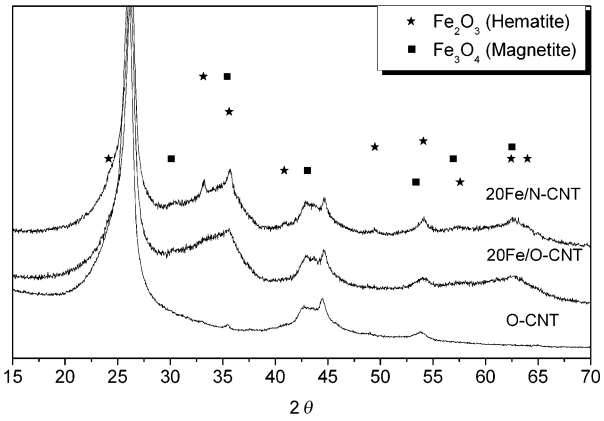


**Figure 1.** XRD patterns of the unloaded oxygen-functionalized CNTs and of the nitrogen and oxygen-functionalized CNTs loaded with 20% Fe.

## Results and Discussion

### Characterization of the catalyst precursor

Summarized in Table 1 are the results of the atomic absorption spectroscopy analysis of the synthesized catalysts with rather similar iron loadings for both supports. The differences between the expected and the obtained iron amount are caused by the ill-defined stoichiometry of the used iron precursor, and the small iron amount observed for the unloaded CNTs results from the residual growth catalyst, which was shown to be inactive in CO hydrogenation under the used reaction conditions.

**Table 1.** Iron content, specific surface areas (BET), and derived iron particle size ($d_{BET}$).

| Catalyst | %Fe | BET [$m^2 g^{-1}$] | BET [$m^2 g_{Fe}^{-1}$] | $d_{BET}$ [nm] |
|---|---|---|---|---|
| unloaded CNTs | 0.97 | 34 | | |
| 20Fe/N-CNT | 17.7 | 86 | 294 | 3.9 |
| 20Fe/O-CNT | 17.9 | 110 | 425 | 2.7 |
| 40Fe/N-CNT | 34.5 | 120 | 249 | 4.6 |
| 40Fe/O-CNT | 35.9 | 126 | 256 | 4.5 |

The unloaded CNTs had a specific surface area of 34 $m^2 g^{-1}$, which increased up to 120 and 126 $m^2 g^{-1}$ owing to the deposition of 40 wt% Fe on N-CNTs and O-CNTs, respectively. This strong increase is assumed to be caused mainly by the deposition of a huge amount of iron oxide nanoparticles, which contribute to the overall specific surface area. Accordingly, average particle sizes between 2.7 and 4.6 nm (Table 1) were obtained by assuming spherical hematite particles.

The XRD patterns of the 20Fe/O-CNT, 20Fe/N-CNT, and unloaded O-CNT samples are shown in Figure 1. Three new very broad peaks at $\theta = 36.0$, 49.5, and 62.5° attributable to the deposition of iron oxide are evident. These very broad and asymmetric peaks make it impossible for us to assign a defined iron phase and to apply the Scherrer equation to obtain the particle size. Nevertheless, it is reasonable to assume that these peaks originate from either hematite or magnetite and are indicative of particles in the low nanometer range (<10 nm). A closer comparison of both iron samples revealed slight differences. For the 20Fe/N-CNT sample, some sharp but very small peaks of hematite superimposed on the broad peaks are present, which originate from a few larger hematite particles. Considering this result, the difference of 1.2 nm between $d_{BET,Fe/O-CNT}$ and $d_{BET,Fe/N-CNT}$ may be attributed to an averaging effect of the bimodal particle size distribution of iron oxide nanoparticles supported on N-CNTs. Therefore, both supported iron samples can be considered as nearly identical with respect to the iron particle size.

Temperature-programmed reduction in hydrogen ($H_2$ TPR) experiments were used to elucidate the reduction properties of the calcined samples. The reduction profiles for the samples 20Fe/O-CNT and 20Fe/N-CNT are shown in Figure 2, which are nearly identical. The $H_2$ consumption during the TPR experiments should be caused mainly by iron oxide reduction. Additionally, the oxygen-containing functional groups on the CNT support are reduced under the TPR conditions.[19] However, the amount of surface oxygen species on O-CNTs is much lower compared to the amount of oxygen present in the deposited iron oxide nanoparticles. Therefore, their influence on the $H_2$ consumption profiles can be neglected. The TPR profiles of both catalysts demonstrate three different maxima, which

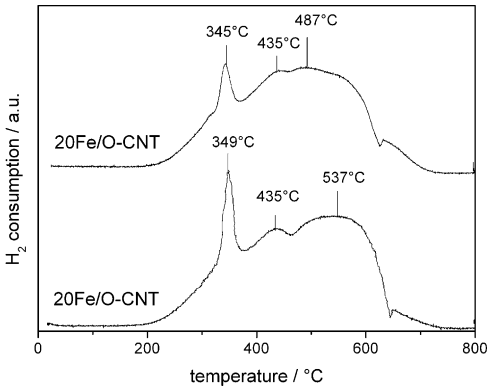


**Figure 2.** TPR profiles of the N-CNTs and O-CNTs loaded with 20% Fe.

  

suggest a stepwise reduction of iron oxide nanoparticles [Eq. (1)]:[20,21]

$$Fe_2O_3 \rightarrow Fe_3O_4 \rightarrow FeO \rightarrow Fe \quad (1)$$

The first peak at 350 °C can be assigned to the reduction of $Fe_2O_3$ to $Fe_3O_4$. Its onset is at about 200 °C, which points to an enhanced reducibility of very small CNT-supported hematite particles. The second peak between 400 and 500 °C may be related to the reduction of $Fe_3O_4$ to FeO, and the last peak at 500–650 °C can be assigned to the subsequent reduction of FeO to Fe. The presence of metastable FeO is supported by the XRD results obtained by Bao and co-workers.[15] They reduced iron oxide supported on O-CNTs in $H_2$ monitoring phase changes by means of in situ XRD analysis as a function of temperature. The presence of FeO was observed from 450 to 620 °C, which is in very good agreement with our results. However, the reduction kinetics of iron oxides is strongly decelerated by the produced water vapors.[22] A quantitative analysis of the TPR profile, assuming all iron in the catalysts to be hematite and a 1.5 stoichiometry of reduction to iron, indicates that both samples were completely reduced in the TPR experiments.

The TEM analysis of N-CNTs and O-CNTs loaded with 20% Fe after calcination (Figure 3) revealed iron oxide particle diameters of approximately 8 nm, with rather sharp particle size distributions, which is in good agreement with the results obtained by means of XRD analysis, whereas the particle sizes estimated based on $N_2$ physisorption are somewhat smaller. Bao and co-workers[15] and Dalai and co-workers[16] positioned iron nanoparticles either inside or outside their CNTs, whereas we used high amounts of ammonium iron citrate solution and long CNTs to prevent iron deposition inside the CNTs. Correspondingly, the TEM analysis of the fresh (Figure 3) and used catalysts (Figure 5) revealed well-dispersed iron particles mainly outside the CNTs.

In summary, the results of all characterization methods indicate that rather similar CNT-supported iron oxide samples were obtained and that surface activation has no influence on the resulting oxide catalyst precursor. It might, therefore, be expected that the catalytic properties of both catalysts should be almost identical under FTS conditions.

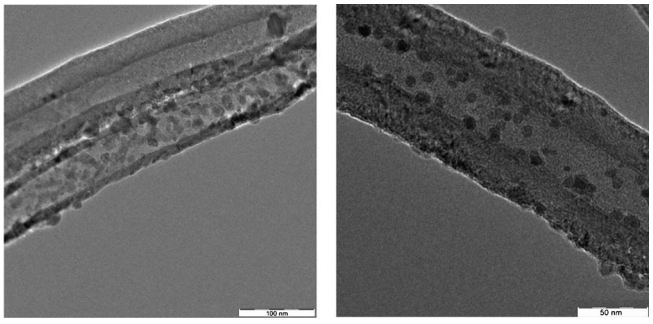


**Figure 3.** TEM micrographs of N-CNTs (left) and O-CNTs (right) loaded with 20% Fe after calcination. The scale bars represent 100 nm and 50 nm, respectively.

### Characterization of the used catalysts

Shown in Figure 4 the XRD patterns of O-CNTs and N-CNTs loaded with 20% Fe after 50 h time on stream under FTS conditions. The dominating iron phase in both catalysts is the

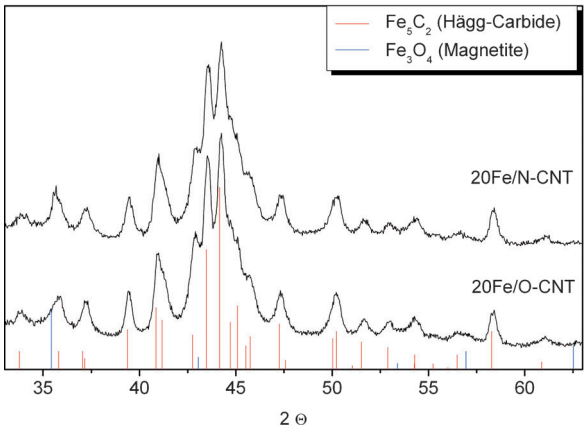


**Figure 4.** XRD patterns of N-CNTs and O-CNTs loaded with 20% Fe after 50 h time on stream under FTS conditions.

Hägg carbide ($Fe_5C_2$), which is known to be highly catalytically active for FTS.[23] Additionally, the width of reflections of the used catalysts was found to be considerably lower, and just a minor amount of magnetite was detected. This is quite surprising because several groups found significant amounts of $Fe_3O_4$, magnetite, in conventional supported and unsupported catalysts used in long-term FTS studies.[24–26] Clearly, the application of an oxygen-free carbon-based support favors the formation of iron carbides. The calculation of the average particle sizes for the used catalysts based on the Scherrer equation resulted in average diameters of 20 and 22 nm for N-CNT- and O-CNT-supported catalysts, respectively.

The TEM results illustrated in Figure 5 reveal that the $Fe_5C_2$, iron carbide, nanoparticles formed during FTS are mainly spherical and located on the outer surface of the CNTs.

A particle size distribution count of 850 particles for each sample was derived (Figure 6). By comparing the average particle sizes, a difference of 3.6 nm between the 20Fe/N-CNT (22.7 nm) and 20Fe/O-CNT (26.3 nm) samples was derived,

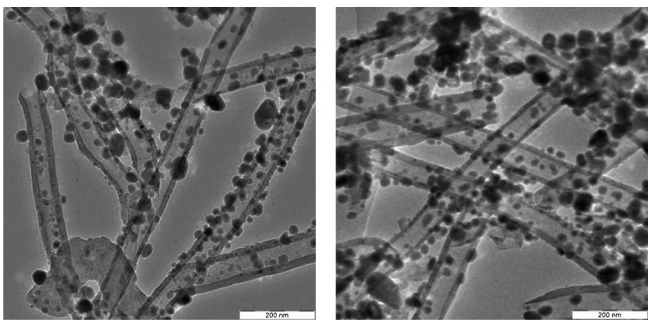


**Figure 5.** TEM micrographs of N-CNTs (left) and O-CNTs (right) loaded with 20% Fe after reaction. The scale bars represent 200 nm.

  

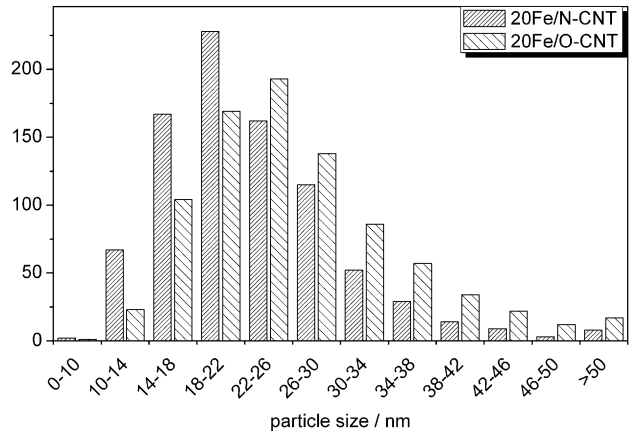


**Figure 6.** Particle size distributions of the used catalysts.

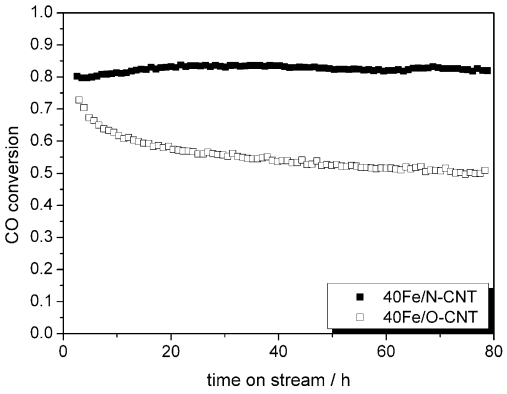


**Figure 8.** CO conversion as a function of time on stream for the 40% Fe catalysts. Reaction conditions: 340 °C, 25 bar, $H_2/CO = 1$, 833 sccm $g^{-1}$ $min^{-1}$.

which is in good agreement with the results obtained from the XRD analysis. Assuming all iron to be present as $Fe_5C_2$, specific $Fe_5C_2$ surface areas of 34 and 30 $m^2 g^{-1}$ for the 20Fe/N-CNT and 20Fe/O-CNT catalysts, respectively, were calculated corresponding to a difference of 12% for the available active sites.

### Catalytic testing

The catalytic activity expressed as the degree of CO conversion is shown in Figures 7 and 8 as a function of time on stream. FTS was performed at 340 °C at a pressure of 25 bar (absolute), a ratio of $H_2/CO = 1$, and a total volumetric flow rate of 833 sccm $g^{-1}$ $min^{-1}$. The initial degree of conversion values after 3 h time on stream were nearly identical, followed by a period of deactivation for all catalysts ending at a steady-state conversion level. For both O-CNT catalysts, deactivation was more pronounced. The iron-based degree of CO conversion levels under steady-state conditions are summarized in Table 2. Clearly, the nitrogen functionalization resulted in a remaining activity twice as high as for iron supported on O-CNTs. In addition, we tested iron supported on nonfunctionalized CNTs, which was found to be nearly inactive, demonstrating the role of efficient functionalization.

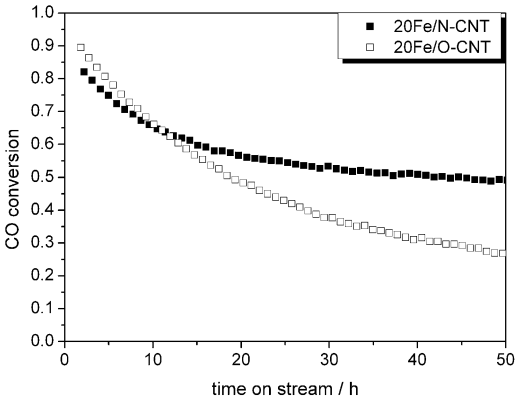


**Figure 7.** CO conversion as a function of time on stream for the 20% Fe catalysts. Reaction conditions: 340 °C, 25 bar, $H_2/CO = 1$, 833 sccm $g^{-1}$ $min^{-1}$.

**Table 2.** CO conversion, weight-related rate, $CO_2$ yield, chain growth probability, and methane and olefin selectivities of iron catalysts.[a]

| Parameter | Catalyst | | | | | |
|---|---|---|---|---|---|---|
| | 20Fe/ N-CNT | 20Fe/ O-CNT | 40Fe/ N-CNT | 40Fe/ O-CNT | Fe[a] powder | K/Fe[b] powder |
| $X_{CO}$ [%] | 48.3 | 26.5 | 81.9 | 50.0 | 97.0 | 97.2 |
| Activity [$\mu mol_{CO}\, g_{Fe}^{-1} h^{-1}$] | 46.1 | 25.0 | 42.3 | 23.1 | 0.3 | 0.3 |
| $Y_{CO_2}$ [%] | 22.5 | 11.5 | 40.3 | 24.0 | 47.0 | 48.0 |
| $A$ | 0.45 | 0.44 | 0.50 | 0.50 | 0.47 | 0.59 |
| $S_{CH_4}$ | 0.09 | 0.06 | 0.11 | 0.08 | 0.14 | 0.12 |
| $C_{2=}-C_{6=}/C_2-C_6$ | 0.70 | 0.90 | 0.72 | 0.92 | 0.55 | 0.78 |

[a] Reaction conditions: 340 °C, 25 bar (absolute), $H_2/CO = 1$, 833 sccm $g^{-1}$ $min^{-1}$; [b] Fe powder from Ref. [27], 16.6 sccm $g^{-1}$ $min^{-1}$; [c] 0.20% K/Fe powder from Ref. [27], 16.6 sccm $g^{-1}$ $min^{-1}$.

The selectivities are summarized in Table 2. The chain growth probability $\alpha$ was low for all catalysts, which was expected because of the applied high-temperature FTS conditions. All catalysts showed excellent olefin selectivities [$S(C_3-C_6) > 85\%$] in the short-chain region, in which the O-CNT-supported iron catalysts had a slightly higher olefin selectivity (Figure 9). This is quite remarkable, because no conventional olefin promoter was present. A comparison of these results with those obtained using a bulk iron catalyst[27] under nearly identical conditions reveals an increase in olefin selectivity from 55 to 78%. An increase in olefinicity for these conventional catalysts had to be achieved by adding a potassium salt as promoter. Unfortunately, the presence of the potassium promoter also resulted in an increase in the growth probability $\alpha$ from 0.47 to 0.59, which is a severe disadvantage when the aim is to obtain short olefins. In contrast, the N-CNT and O-CNT catalysts showed very moderate growth probabilities (0.44–0.50). Consequently, the use of the CNT-supported iron catalysts allows us to reach high olefin selectivities without changing the growth probabilities.

All catalysts were found to have significant methane selectivities of 6–11% (Table 2), which is a consequence of the

  

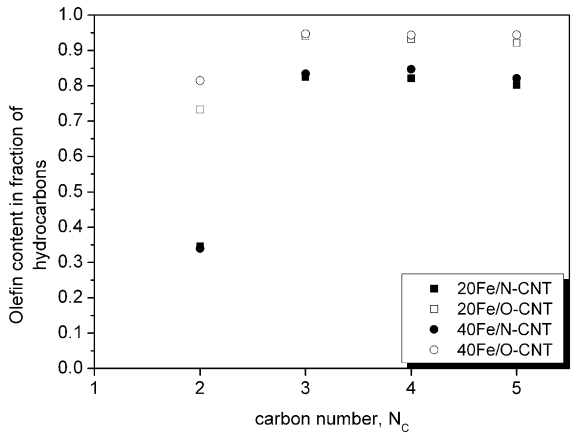


**Figure 9.** Olefin selectivity in the fraction of hydrocarbons as a function of the carbon number.

chosen reaction conditions. This methanation tendency was more pronounced for the N-CNT-supported iron catalysts. It has to be taken into account that the selectivities were obtained at different degrees of conversion. Comparing these results with a bulk iron catalyst,[27] the methanation tendency was found to strongly suppressed by supporting iron on CNTs.

The formation of $CO_2$ indicates a high water gas shift (WGS) activity for all catalysts. This is quite surprising, because only small amounts of magnetite catalyzing the WGS reaction[28] were detected in the used catalysts. It is possible that already a small amount of highly active and presumably X-ray amorphous magnetite particles are able to catalyze the WGS reaction.

A comparison of the catalytic properties of the O-CNT- and N-CNT-supported iron catalysts reveals that the use of O-CNTs as support results in higher olefin selectivities and a lower methanation tendency (Table 2). However, the stability of these catalysts was not as high as that of the N-CNT-supported catalysts. To the best of our knowledge, the 40Fe/N-CNT catalyst is the first CNT-based catalyst that is able to achieve a high and constant degree of CO conversion for a period of 80 h time on stream under the demanding high-temperature FTS conditions.

The $Fe_5C_2$ surface areas derived from the average particle sizes differed only by 12% for the N-CNT- and O-CNT-supported catalysts with 20% Fe, whereas the difference in activity was nearly 50%. Therefore, it can be concluded that the N-CNT-supported iron catalyst has a higher intrinsic activity. De Jong and co-workers[29] observed an increasing turnover frequency (TOF) for cobalt catalysts supported on carbon nanofibers by increasing the cobalt particle size up to 6 nm. As $Fe_5C_2$ nanoparticles were larger than 20 nm, a particle size effect on the intrinsic activity is not considered likely. Abate et al.[30] showed that Pd loaded on N-doped nanocarbon had a higher catalytic activity in the direct synthesis of $H_2O_2$ from $H_2$ and $O_2$. They assumed an electronic effect caused by pyridinic nitrogen sites to be responsible for this activity increase. Again, this is not considered likely for $Fe_5C_2$ nanoparticles with diameters larger than 20 nm. Günter et al.[31] investigated the influence of microstructural strain on the catalytic activity of Cu/ZnO methanol synthetic catalysts. They were able to correlate high TOFs for methanol with a large degree of microstrain in copper nanoparticles. It can be speculated that the deposition of $Fe_5C_2$ nanoparticles on the curved CNT surfaces induces microstructural strain, which modifies the exposed surfaces and may even be larger for N-functionalized CNTs. The dissolution of nitrogen in $Fe_5C_2$ nanoparticles may also contribute to the strain. Further studies using XRD line profile analysis and HRTEM are in progress, which also include the addition of promoters, such as potassium.[27,28,32,33]

## Conclusions

Iron nanoparticles supported on oxygen- and nitrogen-functionalized carbon nanotubes (O-CNTs and N-CNTs) were synthesized by impregnation and applied in high-temperature FTS. The obtained catalysts showed excellent olefin selectivities, moderate methanation tendency, low growth probabilities, and good stabilities. Compared with conventional bulk iron FT catalysts, the CNT-supported catalysts favor the formation of short-chain olefins without requiring additional promoters.

Nitrogen- and oxygen-containing functional groups were found to act as efficient anchoring sites for the deposited iron nanoparticles. After reaction, $Fe_5C_2$ was detected with particle sizes of 23 and 26 nm on O-CNTs and N-CNTs, respectively.

The nitrogen functionalization resulted in a higher intrinsic activity; for N-CNTs loaded with 40% Fe, a high and constant degree of CO conversion was obtained for a period of 80 h time on stream under industrially relevant conditions.

## Experimental Section

### Catalyst preparation

CNTs with inner diameters of 20–50 nm and outer diameters of 70–200 nm were obtained from Applied Sciences Inc. (Ohio, USA). Prior to use as support, the CNTs were partially oxidized by means of nitric acid vapor treatment at 200 °C for 24 h, which is reported to be highly effective for the oxygen functionalization of CNTs.[34] To introduce N-containing functional groups, one half of the O-CNT batch was loaded into a tubular quartz reactor with an inner diameter of 20 mm. The sample was treated at 400 °C for 6 h in flowing ammonia, with a flow rate of 25 sccm $min^{-1}$ (10 vol% $NH_3$ in He), which yielded nitrogen-functional groups.[35] As-received O-CNT and N-CNT samples were loaded with iron according to the ammonium iron citrate method described by Boot et al.[36] For this purpose, O-CNTs and N-CNTs were suspended in an ammonium iron citrate solution of predetermined iron amount corresponding to an iron loading of 20 wt% (20Fe/O-CNT and 20Fe/N-CNT) or 40 wt% (40Fe/O-CNT and 40Fe/N-CNT). The mixture was dried by circulating air at 50 °C overnight in a drying furnace. Calcination was performed in dynamic air (100 sccm $min^{-1}$) with a heating rate of 2 °C $min^{-1}$ up to 300 °C and holding this temperature for 90 min.

  

### Catalyst characterization

Atomic absorption spectroscopy (AAS) was used for elemental analysis. Static nitrogen physisorption experiments were performed in a modified Autosorb-1C setup (Quantachrome). All samples were pretreated at 200 °C for 2 h under dynamic vacuum conditions. Data were analyzed according to the Brunauer–Emmett–Teller (BET) equation by assuming that the area covered by a nitrogen molecule equals 0.162 $nm^2$. Transmission electron microscopy (TEM) analysis was performed with a Hitachi H-8100 microscope (200 kV, $LaB_6$ filament). The samples were prepared by dispersing the powder material in ethanol and dropping the solution on a carbon-coated Au grid. X-ray diffraction (XRD) patterns were recorded in the $2\theta$ range 15–75° (a step width of 0.030°) with a Panalytical MPD diffractometer using $CuK_\alpha$ radiation, 0.5° divergent and antiscatter slits, a 0.2 mm high receiving slit, incident and diffracted beam 0.04 rad soller slits, and a secondary graphite monochromator. Temperature-programmed reduction in hydrogen ($H_2$ TPR) was performed by heating approximately 60 mg of samples to 800 °C with a ramp rate of 10 °C $min^{-1}$ in a gas mixture of 4.36% $H_2$ in Ar using a flow rate of 84.1 sccm $min^{-1}$.

### Catalytic tests

The as-received catalysts were pretreated in a fixed-bed microreactor by reduction in $H_2$ at 380 °C and 25 bar for 8 h with a heating rate of 2 °C $min^{-1}$. Afterward, the reactor was cooled to the reaction temperature of 340 °C. Syngas (45% CO, 45% $H_2$, 10% Ar) was passed over the catalyst, with a specific flow rate of 833 sccm $g^{-1}$ $min^{-1}$ at 340 °C and a pressure of 25 bar (absolute). Online gas analysis was performed with a QP2010 GC–MS (Shimadzu) using argon as internal standard to ensure accurate mass balances.

## Acknowledgements

*Fruitful discussions with Hans Schulz and Robert Schlögl are gratefully acknowledged.*

**Keywords:** doping · nanotubes · Fischer–Tropsch · iron · olefin synthesis

[1] M. J. A. Tijmensen, A. P. C. Faaij, C. N. Hamelincka, M. R. M. van Hardeveld, *Biomass Bioenergy* **2002**, *23*, 129 – 152.
[2] M. E. Dry, *Appl. Catal. A* **1996**, *138*, 319 – 344.
[3] M. E. Dry in *Handbook of Heterogeneous Catalysis, Vol. 2* (Eds.: G. Ertl, H. Knözinger, J. Weitkamp), Wiley-VCH, Weinheim **2008**, pp. 2965 – 2994.
[4] M. E. Dry, *Catal. Today* **2002**, *71*, 227 – 241.
[5] D. B. Bukur, X. Lang, D. Mukesh, W. H. Zimmerman, M. P. Rosynek, C. Li, *Ind. Eng. Chem. Res.* **1990**, *29*, 1588 – 1599.
[6] H. Schulz, *Appl. Catal. A* **1999**, *186*, 3 – 12.
[7] H-J. Jung, M. A. Vannice, L. N. Mulay, R. M. Stanfield, W. N. Delgass, *J. Catal.* **1982**, *76*, 208 – 224.
[8] H-J. Jung, P. L. Walker, Albert Vannice, *J. Catal.* **1982**, *75*, 416 – 422.
[9] J. Venter, M. Kaminsky, G. L. Geoffroy, M. A. Vannice, *J. Catal.* **1987**, *105*, 155 – 162.
[10] J. Venter, M. Kaminsky, G. L. Geoffroy, M. A. Vannice, *J. Catal.* **1987**, *103*, 450 – 465.
[11] J. Venter, A. A. Chen, J. Phillips, G. L. Geoffroy, M. A. Vannice, *J. Catal.* **1989**, *119*, 451 – 466.
[12] E. van Steen, F. F. Prinsloo, *Catal. Today* **2002**, *71*, 327 – 334.
[13] M. C. Bahome, L. J. Jewell, D. Hildebrandt, D. Glasser, N. J. Coville, *Appl. Catal. A* **2005**, *287*, 60 – 67.
[14] U. Graham, A. Dozier, R. Khatri, M. Bahome, L. Jewell, S. Mhlanga, N. Coville, B. Davis, *Catal. Lett.* **2009**, *129*, 39 – 45.
[15] W. Chen, Z. Fan, X. Pan, X. Bao, *J. Am. Chem. Soc.* **2008**, *130*, 9414 – 9419.
[16] R. M. M. Abbaslou, A. Tavassoli, J. Soltan, A. K. Dalai, *Appl. Catal. A* **2009**, *367*, 47 – 52.
[17] R. Chetty, S. Kundu, W. Xia, M. Bron, W. Schuhmann, V. Chirila, W. Brandl, T. Reinecke, M. Muhler, *Electrochim. Acta* **2009**, *54*, 4208 – 4215.
[18] H. Xiong, M. Moyo, M. Rayner, L. Jewell, D. Billing, N. Coville, *ChemCatChem* **2010**, *2*, 514 – 518.
[19] S. Kundu, Y. Wang, W. Xia, M. Muhler, *J. Phys. Chem. C* **2008**, *112*, 16869 – 16878.
[20] W. Ma, E. L. Kugler, J. Wright, D. B. Dadyburjor, *Energy Fuels* **2006**, *20*, 2299 – 2307.
[21] R. M. M. Abbaslou, J. Soltan, A. K. Dalai, *Appl. Catal. A* **2010**, *379*, 129 – 134.
[22] O. J. Wimmers, P. Arnoldy, J. A. Moulijn, *J. Phys. Chem.* **1986**, *90*, 1331 – 1337.
[23] J. Xu, C. H. Bartholomew, *J. Phys. Chem. B* **2005**, *109*, 2392 – 2403.
[24] T. Riedel, H. Schulz, G. Schaub, K. Jun, J. Hwang, K. Lee, *Top. Catal.* **2003**, *26*, 41 – 54.
[25] S. Li, G. D. Meitzner, E. Iglesia, *J. Phys. Chem. B* **2001**, *105*, 5743 – 5750.
[26] A. Sarkar, D. Seth, A. Dozier, J. Neathery, H. Hamdeh, B. H. Davis, *Catal. Lett.* **2007**, *117*, 1 – 17.
[27] B. Graf, H. J. Schulte, M. Muhler, *J. Catal.* **2010**, *276*, 66 – 75.
[28] G. P. van der Laan, A. A. C. M. Beenackers, *Catal. Rev. Sci. Eng.* **1999**, *41*, 255 – 318.
[29] G. L. Bezemer, J. H. Bitter, H. P. C. E. Kuipers, H. Oosterbeek, J. E. Holewijn, X. Xu, F. Kapteijn, A. J. van Dillen, K. P. de Jong, *J. Am. Chem. Soc.* **2006**, *128*, 3956 – 3964.
[30] S. Abate, R. Arrigo, M. E. Schuster, S. Perathoner, G. Centi, A. Villa, D. Su, R. Schlögl, *Catal. Today* **2010**, *157*, 280 – 285.
[31] M. M. Günter, T. Ressler, B. Bems, C. Büscher, T. Genger, O. Hinrichsen, M. Muhler, R. Schlögl, *Catal. Lett.* **2001**, *71*, 37 – 44.
[32] B. Graf, M. Muhler, *Phys. Chem. Chem. Phys.* **2011**, *13*, 3701 – 3710.
[33] E. Schwab, A. Weck, J. Steiner, K. Bay, *OIL GAS* **2010**, *36*, 44 – 47.
[34] W. Xia, C. Jin, S. Kundu, M. Muhler, *Carbon* **2009**, *47*, 919 – 922.
[35] S. Kundu, W. Xia, W. Busser, M. Becker, D. A. Schmidt, M. Havenith, M. Muhler, *Phys. Chem. Chem. Phys.* **2010**, *12*, 4351 – 4359.
[36] L. A. Boot, A. J. van Dillen, J. W. Geus, F. R. van Buren, *J. Catal.* **1996**, *163*, 186 – 194.

Received: August 10, 2011
Published online on ■■ ■■, 0000

  

**Syngas on a short-leash:** Unpromoted Fischer–Tropsch iron catalysts supported on oxygen- and nitrogen-functionalized carbon nanotubes (CNTs) are highly active and selective for the production of high-value, short-chain $\alpha$-olefins. Nitrogen functionalization of the CNTs resulted in excellent selectivities compared to those of traditional Fischer–Tropsch catalysts. The scale bar represents 200 nm.

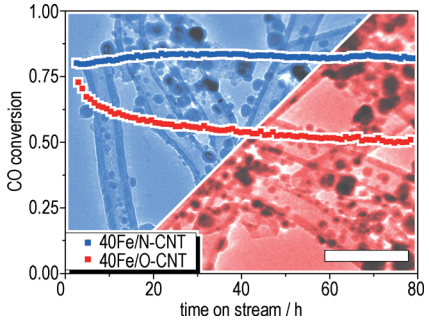


*H. J. Schulte, B. Graf, W. Xia, M. Muhler**

■■ – ■■

**Nitrogen- and Oxygen-Functionalized Multiwalled Carbon Nanotubes Used as Support in Iron-Catalyzed, High-Temperature Fischer–Tropsch Synthesis**

  